www.DeepakPublishing.com

Dearborn, M. et al. (2014): JoSS, Vol. 3, No. 1, pp. 253-264
(Peer-reviewed Article available at www.jossonline.com)

www.JoSSonline.com

A Deployable Membrane Telescope Payload for CubeSats

Michael E. Dearborn[1], Geoff P. Andersen[1], Olha Asmolova[1], Richard L. Balthazor[1], Matthew G. McHarg[1], Heather C. Nelson[1], Trey S. Quiller[1], Gabe R. Wilson[1], Thomas J. Harvey[2], and Thomas W. Murphey[3]

[1] *USAF Academy Department of Physics, Colorado Springs, CO USA*
[2] *MMA Design, LLC, Boulder, CO USA*
[3] *Air Force Research Laboratory, Albuquerque, NM USA*

Abstract

This article reports on the design and development of a deployable membrane telescope suitable for incorporation on 3U CubeSats. When hosting imaging payloads, the size of the primary optic has effectively been limited to the cross section size of the satellite bus. For 1U to 3U CubeSats, this is a diameter of less than 10 cm. To overcome this limitation, cadets and faculty at the US Air Force Academy (USAFA) are currently developing a deployable membrane telescope called Peregrine. Peregrine fits into a 1.5U volume and has a mass of less than 1.4 kg. The telescope includes a 20 cm photon sieve membrane primary optic that is deployed from the end of a CubeSat using a spring-loaded pantograph-based deployment system. A photon sieve (PS) is a diffractive optic that uses a pattern of billions of circular pads with relative size and positioning such that transmitted light though the photon sieve is diffracted to a focal plane array within the CubeSat. The deployable membrane telescope promises the ability to enable missions with a primary optical element that is larger than that of traditional optics, allowing for missions with greater optical resolution.

1. Introduction

The development of technology for the CubeSat industry over the past several years has been impressive. CubeSat capabilities have enabled a wide range of space experiments and missions, ranging from orbital decay studies (Fuller, 2010) to environmental monitoring (Bleier, 2004) to biological missions (Minelli, et al., 2008; Niesel, 2010) to imagers (Simms, 2012). Cadets and faculty at the US Air Force Academy (USAFA) are

Corresponding Author: Michael E. Dearborn - medearborn@yahoo.com
Publication History: Submitted – 09/19/13; Revision Accepted – 04/23/14; Published – 08/14

designing and constructing a deployable membrane solar telescope (Peregrine) that will image the Sun. Although there have been other small satellite missions that have deployed membranes (Katan, 2012; Stohlman, 2013) to the authors' knowledge, this is the first deployable telescope payload for CubeSats. The primary optic of this membrane solar telescope is a photon sieve (PS) - a diffractive optic consisting of billions of tiny circular pads on a transparent polymer substrate. The 20 cm telescope is optimized for H-alpha imaging (656 nm), and is designed to be deployed from a 0.1 m square cross-section, suitable for CubeSats. The 0.2 m-diameter, f/2 primary uses a 20-micron-thick Kapton polyimide with a mass of less than 10 grams. The membrane is pulled flat by a configuration of hexapod lanyards held taut by a triangular pantograph support structure. The membrane, support structure, secondary optics, camera, and associated control electronics are all packaged within 1.5U, and have a mass of less than 1.4 kg.

One purpose of the Peregrine payload is to demonstrate optical membrane technology that can be used on CubeSats for science missions. For example, scientific understanding of the solar atmosphere is currently limited by the fact that high-resolution (sub 0.1 arcsec) images of the Sun have not been captured. It is well known from indirect diagnostics that some of the most important components of the solar atmosphere, including photospheric magnetic flux tubes and the filamentary plasma within coronal loops, are spatially unresolved by any existing space- or ground-based imaging. NASA recognized the fundamental importance of crossing the 0.1-arcsec threshold for solar observations over 20 years ago and embodied this objective in the Solar Optical Telescope mission (Lites, 1991), later renamed the Orbiting Solar Laboratory (OSL). OSL was effectively cancelled in 1991, largely because of cost.

The main obstacle remains the prohibitive cost of a conventional large-aperture (> 1 m) spaceborne solar telescope, with traditional primary optics. The Peregrine payload will demonstrate the technology necessary to enable new imaging science missions, such as solar imaging.

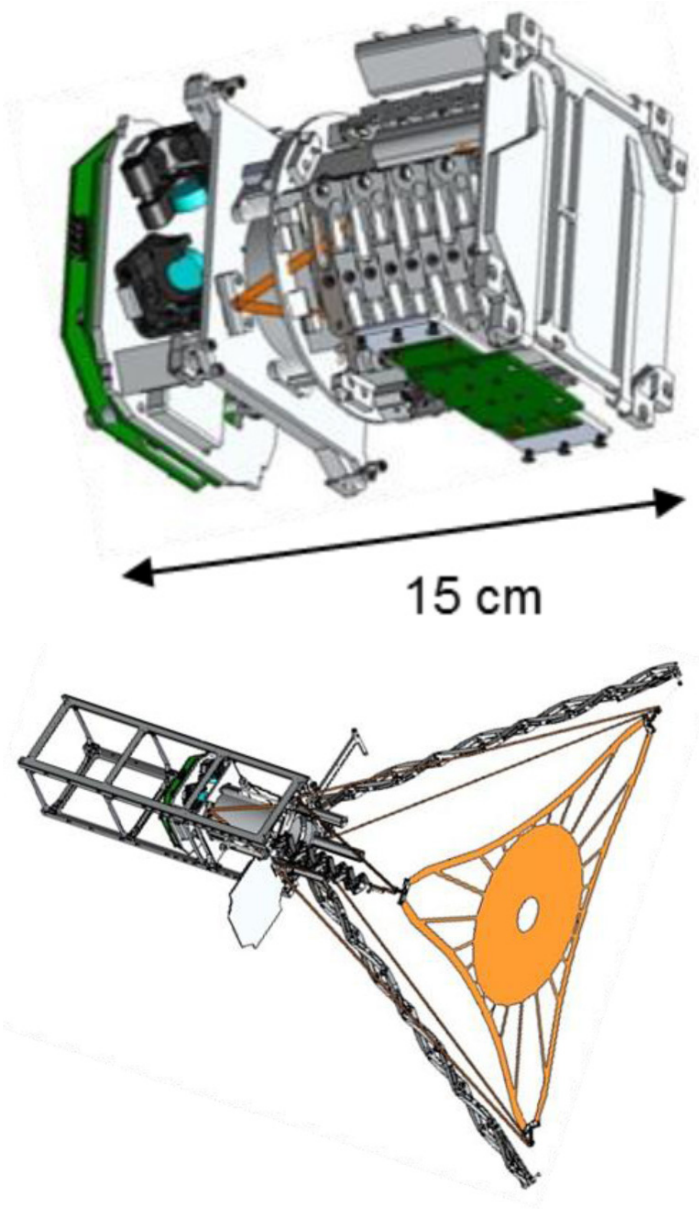

Figure 1. Stowed and deployed Peregrine payload that fits in 1.5 U.

Peregrine (Figure 1) consists of four subsystems: 1) membrane; 2) deployment structure; 3) optical platform (which contains the secondary optics and primary camera); and 4) electronics and software. The membrane and deployment structure subsystems are strongly linked, in terms of overall optical performance of the payload. The following sections address each of the subsystems in turn, along with a section on optical-mechanical modeling of the coupled membrane/deployment structure subsystems.

2. Membrane

The PS is essentially a Fresnel zone plate (FZP) in which the rings have been broken up into many individual circular pads or holes. The FZP uses diffraction to focus incoming light, as opposed to refraction or reflection of traditional lenses or mirrors, respectively (Arsenault, 1968). Figure 2 shows a diffraction-limited image obtained in the laboratory of a 20-cm photon sieve made of quartz. The planned PS is binary in nature and is a phase PS (raised circular pads on a transparent substrate) that is relatively simple to manufacture, but results in a diffraction efficiency in the first order ~30%. Details on the general optical requirements for design of a PS (Andersen, 2005) and the imaging performance of a PS telescope (Andersen, 2007) are discussed elsewhere.

The PS substrate itself must have good thickness uniformity, and for a transmitted wavefront error of λ/10, the thickness of a PS membrane in a polymer with $n = 1.62$ must vary by no more than 0.6 λ. This is a challenging manufacturing issue, but has been addressed by Mantech International. A PS master is fabricated by the photolithographic printing of the optical pattern on chrome-coated glass. This pattern is then copied onto UV curable polyimide film using contact printing. Regions exposed to UV are chemically processed to harden, and unexposed regions are etched away to give a surface relief, phase grating. The depth of each groove is 0.53 microns for H-alpha wavelength.

The flatness, or out-of-plane deformation, requirement of the membrane is proportional to the square of the f-number (f/#) of the membrane, so an f/4 membrane flatness requirement is 16 times easier to meet than an f/1 membrane. So the membrane does not have to be deployed too far from the CubeSat, Peregrine uses an f/2 PS membrane. This requires a minimum of 40 cm of optical path length for optical imaging. For Peregrine, the PS is held 32 cm from the end of the CubeSat, with the remaining optical path length being contained within the CubeSat. The flatness must be maintained to approximately 8 λ. By comparison, the surface requirements for a traditional reflector would be some 80 times more stringent. This easing of the flatness constraint permits the mechanical deployment of a PS to the required optical tolerances.

The optimal focusing capability of the PS depends on the precise positioning of the circular pads, which is proportional to the wavelength of light being imaged and the f-number of the photon sieve. In other words, small wavelengths and f-numbers give more stringent requirements. This then leads to a requirement on the coefficient of thermal expansion of the membrane material, the operational temperature window over which diffraction limiting imaging can be performed, or both.

In-plane deformations are also of concern. It is also important that the PS material properties such as CTE and modulus of elasticity are isotropic and homogeneous over the entire aperture, since expansion or contraction under these conditions leads to in-plane errors that result in a simple error in de-focus, which can be corrected with the translation stage that is included in the Peregrine payload design.

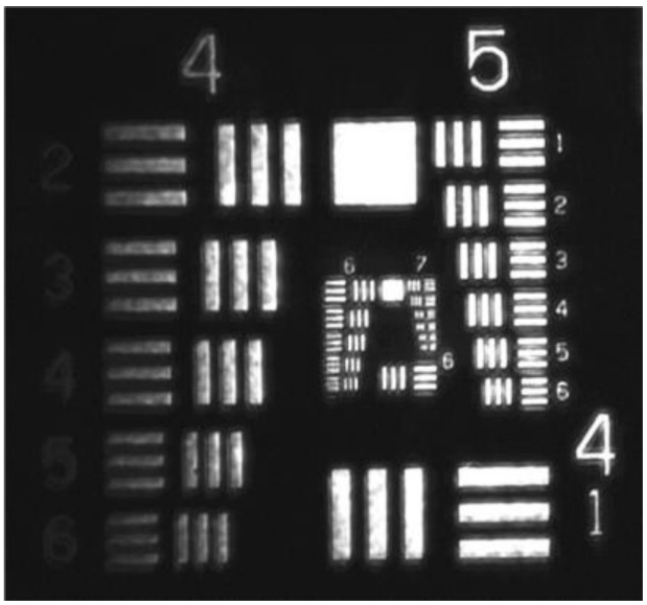

Figure 2. An image of an AF test pattern of the 20 cm PS master which resolves group 7, element 2 indicating diffraction-limited performance.

While the use of PS diffractive primaries simplifies many issues, including mass, volume, and fabrication, there are two trade-offs: decreased optical efficiency (as previously detailed); and large dispersion. Dispersion in the primary results in a change in focal length with the wavelength of the incoming light. This, along with

depth of focus considerations, results in a useable spectral bandwidth that is proportional to the square of the wavelength and the f-number of the membrane. Thus, longer wavelengths and larger f-numbers result in a wider useable spectral bandwidth and the collection of more photons. The photon sieve has a calculated spectral bandwidth of 56 pm.

In addition to the optical design of the PS, consideration must be given to the mechanical design. The mechanical design of the PS material should provide a uniform stress field over the optically patterned region. A uniform stress field will minimize both out-of-plane and in-plane deformations of the PS.

Predictions of the resulting stress field for the mechanical design shown in Figure 4 were made by completing a finite element model using Abaqus software. In addition to the deformations being dependent on the mechanical pattern of the PS (pattern of gores attached to the PS central optically patterned region), they were also dependent on the tension at which the PS was being held at the three attachment points (see Figure 5). Several different mechanical patterns of the PS were examined, at several different tensioning loads. Results of the analysis conducted by AFRL/RV of the chosen mechanical pattern (seen in Figures 4 and 12) held at 0.5 N radial load are shown in Figure 3.

In these figures, it can be seen that the majority of the optically patterned region of the PS for the out-of-plane deformations is less than 3 μm, and for the in-plane deformations less than 0.4 μm. As discussed in Section 6, these deformations allow for acceptable imaging performance.

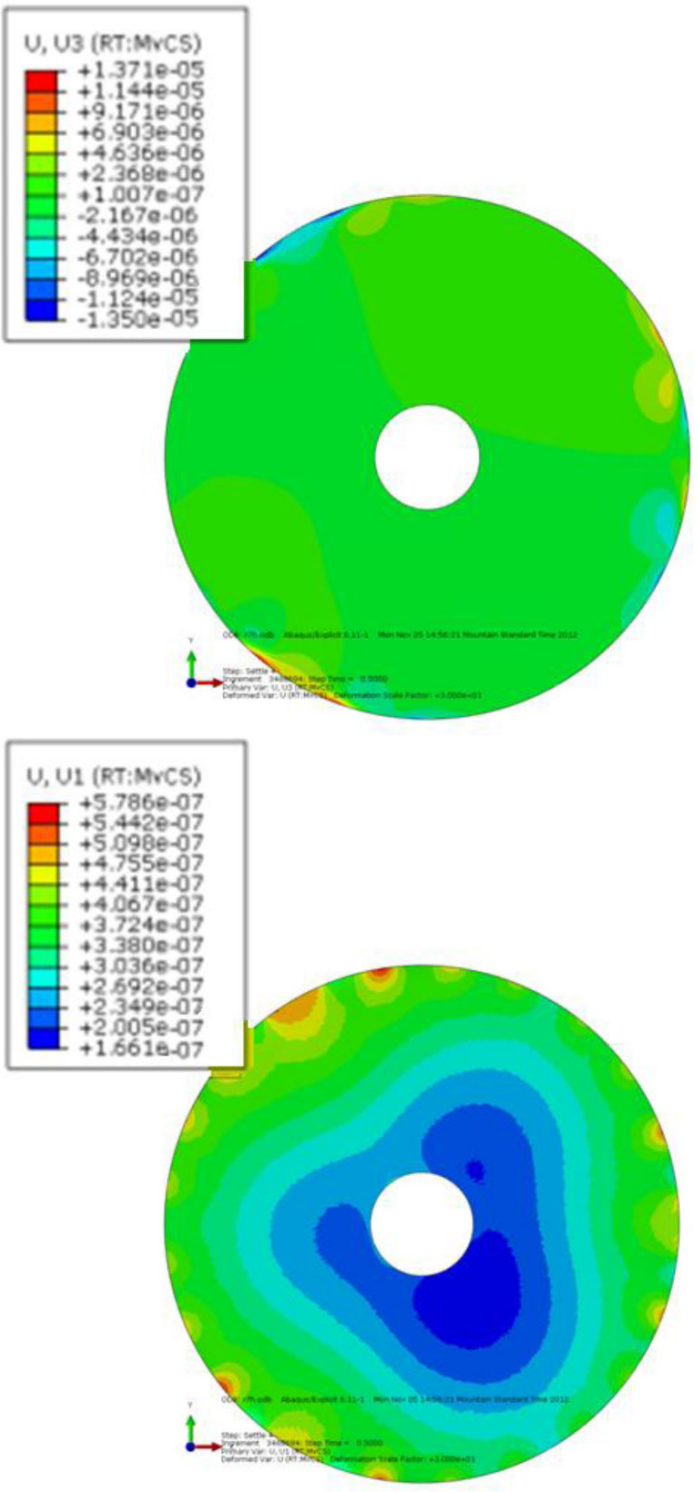

Figure 3. In-plane (top) and out-of-plane (bottom) deformations of the PS under 0.5 N tensions and mechanically patterned as shown in Figure 4. Deformations are shown in meters.

3. Deployment System

In designing a deployment structure to hold the PS, it was necessary to keep in mind total stowed volume, as well as meeting the requirements for PS positioning. The authors examined both spring tape (Footdale, 2013) and pantograph systems (VanHalle, 2013), and selected pantographs based on technical, cost, and schedule constraints. The deployment structure has been previously described (Dearborn, 2012). It consists of three spring-loaded pantographs stowed under compression, with the PS membrane folded inside the

center. The folding of the PS is done in a manner that minimizes the potential for creasing. Once in orbit, the hinged end of panel of FS-7 opens with the use of a melt wire release mechanism, and the pantographs deploy automatically under their loaded spring force. The membrane is pulled to the required flatness by a 0.5 N radial tension provided by the pantographs and upper lanyards that form a tensioned upper hexapod as seen in Figure 4. Table 1 provides some details on the deployment system design margins and materials.

Table 1. Deployment System Design Margins and Materials

Design Margins	**Description**
Factor of safety on yield	1.1
Moving element margin	200%
Assumed maximum coefficient of friction	0.2
Materials	
Molybdenum disulfide thin film lubricants	Everlube 620 Tiolube
Base plate, carriage plate, pantograph links	6061-T6 aluminum
Lower hexapod springs	302 stainless steel
Fasteners	18-8 stainless steel
Pantograph springs	17-7 PH CH900
Rods, axles, axle nuts	303 stainless steel
Upper and lower lanyards	Vectran aramide chord

The positioning of the PS depends critically on the lengths of these lanyards, which form a determinate system. The PS is de-coupled from the pantographs by springs. In order for the pantographs to deploy without interference from the bus structure, they are mounted to a carriage plate that moves the base of the stowed pantographs 7.75 cm from within the bus to the end of the CubeSat. The carriage plate positioning is also critical for optical positioning of the PS, and is held in place by a second, tensioned lower hexapod. The tension for the lower hexapod is provided by springs that also provide the spring force for the movement of the carriage plate. The pantographs have a simple deployment constraint that prevents them from extending up and out from the axis of the CubeSat until after they have cleared the sides of the CubeSat with the movement of the carriage plate. In effect the deployment system is a double deployment. First, the lower hexapod is formed, followed by the formation of the upper hexapod.

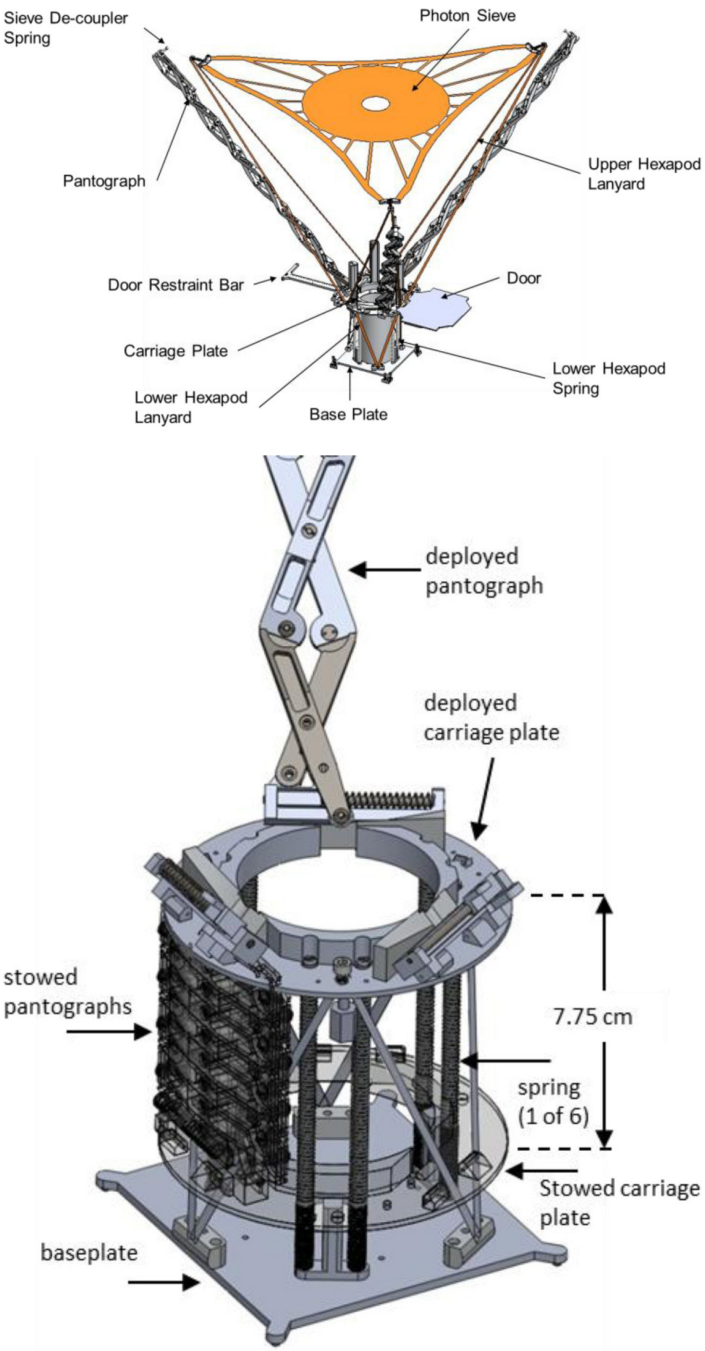

Figure 4. CAD drawing (top) showing Peregrine's double hexapod structure. Superimposed CAD drawing (bottom) showing the stowed configuration (transparent) and deployed (solid) configuration, of the carriage plate and pantographs. (Some parts have been omitted for clarity.)

The PS is folded and stored in a cylinder that is 5 cm in diameter and 7.8 cm tall. The cylinder is anchored

to the deployment structure baseplate and located inside the three stowed pantographs (see Figure 6).

An analog commercial camera (Lawmate CM-SS40) set in the top corner of the CubeSat will be used to take images of the membrane deployment. The camera is a cylinder of less than 5 mm diameter and 43 mm long. The Lawmate will collect images at 19 frames per second, and will be able to confirm that the membrane has deployed without tangling and that there are no tears or major creases. It cannot be used to determine if the membrane was deployed to the correct optical position.

3.1 Deployment Testing

It order to test the deployment of the PS, a series of zero-g deployments funded by the Space Test Program were accomplished on a NASA contracted zero-g aircraft. During the zero-g flight, the Peregrine experiment was deployed a total of six times. Each of the deployments was captured on the high speed cameras, as well as with the standard speed video camera. From analysis of successful deployments, it was found that there was no significant net linear or angular motion of Peregrine after deployment. This was expected, since the only external force on Peregrine was drag from air resistance.

Also noted was that the maximum acceleration on the membrane tips did not exceed 0.8 g. The authors believe the reason for this low acceleration is that as the membrane deploys, rather than "snapping" open, it unwinds as it comes out of the cylinder in which it is initially stored (see Figure 6).

The success of the zero-g testing of the deployment structure gives high confidence of successful deployment on-orbit. A full discussion of the zero-g test and results will be published in a separate paper.

4. Optical Platform

Peregrine contains secondary optics that collimate the beam for transmission through a narrowband filter, as well as changing the effective f-number of the system to f /10. The final focused beam is reflected off three fold mirrors to a 10-bit monochrome CCD camera

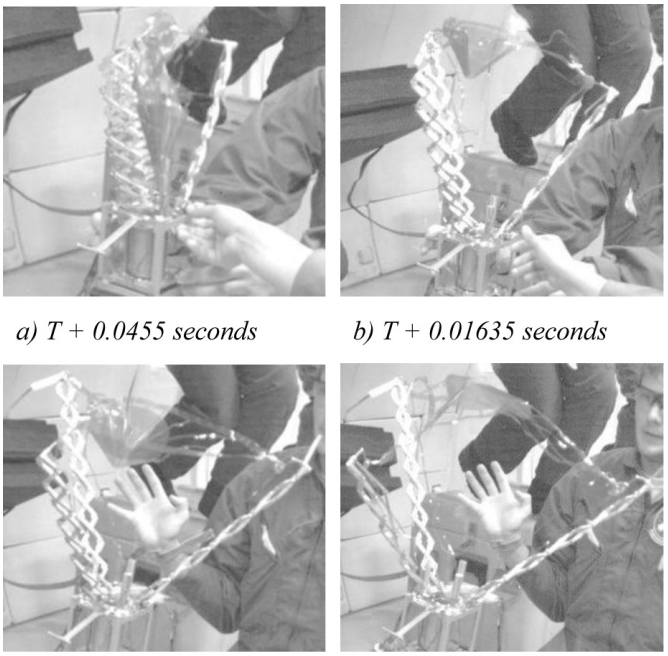

a) T + 0.0455 seconds *b) T + 0.01635 seconds*

c) T + 0.4365 seconds *d) T + 0.5675 seconds*

Figure 5. Unfolding of the PS during zero-g deployment. Note that total time to deploy is between 0.5 and 1 second. T represents the time when the door was freed to open.

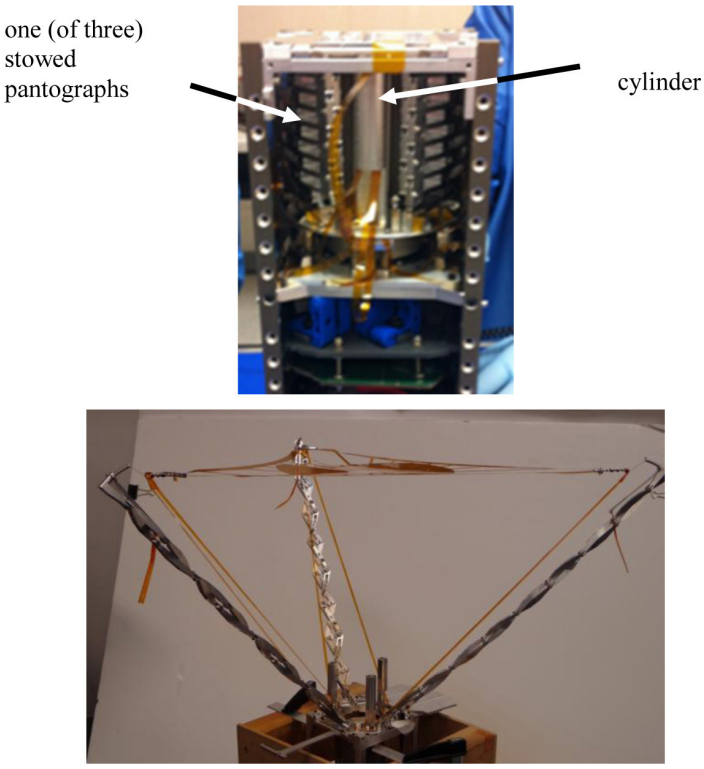

Figure 6. Images of the stowed (top) and deployed (bottom) support structure with membrane. You can see two of the stowed pantographs in the top picture. The PS is stowed in a cylinder that is between the stowed pantographs.

made by Sentech. A vacuum-rated mechanical translation stage with encoder was also used for focusing. This is a commercial product built by Micronix USA, providing 8 mm of travel with a 1.5 nm step size. The translation stage allows for changes in de-focus due to on-orbit thermal effects (expansion and contraction) of the PS optical pattern. All of the secondary optics, translation stage, and main camera fit within a 3.5 cm height on an optical platform that is approximately 9.4 cm square. A picture and CAD model of the optical platform, which is located directly beneath, and attached to, the deployment assembly is shown in Figure 7. The optical layout is shown in Figure 8.

Radiometric analysis shows that there will be more than sufficient light to obtain images of the Sun at an acceptable signal-to-noise. The present analysis takes into account use of an Andover narrow-band filter to eliminate the majority of non-focused light at the focal plane array (FPA) of the camera. The filter has a FWHM of 1.5 angstroms and peak transmission of 35%. Finally, using Zemax, an analysis was performed indicating that stray light represented less than 1.25% of the total energy at the FPA. Overall performance characteristics for the Peregrine telescope are given in Table 2.

One of three fold mirrors is fixed, and the other two are commercial optical mounts. The secondary optics were optically aligned using an f/2 lens in place of the PS. The mirror mounts were then potted in place and the optical alignment was re-tested, successfully ensuring that the potting process did not have an adverse effect on imaging performance. The optical platform assembly for the launch vibration environment was then tested in three axes (NASA GEVS), optically testing between each axis. The optical platform is attached to the base plate of the deployment assembly at three points with pin and bolt attachments.

Table 2. Performance Characteristics of the Peregrine PS Telescope.

Telescope characteristic	**Value**
Angular resolution	4 μrad
Field of view	0.013 degrees
SNR	>20
Solar resolution	630 km

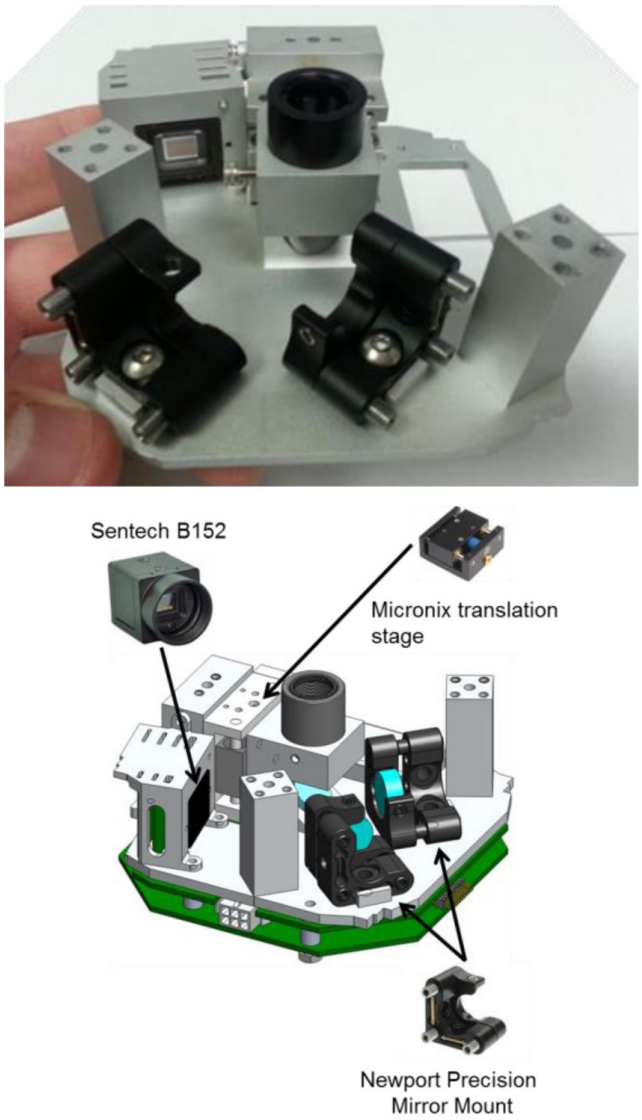

Figure 7. CAD model (bottom) and picture (top) of the optical platform prototype containing the main camera, translation stage, fold mirrors, and secondary optics. The secondary optics cannot be seen since they are mounted in the optical tube.

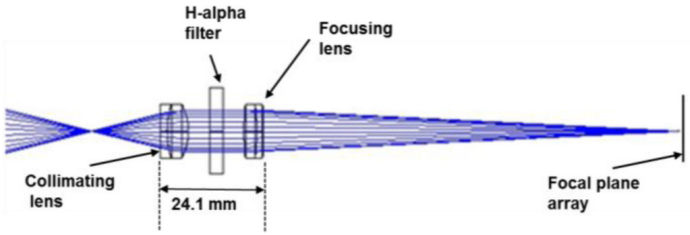

Figure 8. The Peregrine secondary optics with focused light coming from the PS to the left (not shown) passing through two lenses and the filter. The collimated beam is approximately 10mm in diameter, and the final focal distance from the second lens to the camera focal plane is about 100mm. The three fold mirrors after the final lens are not shown.

5. Electronics and Software

The payload electronics must provide command and control (C&C) of the payload, as well as data handling. C&C requirements include the operation of the main camera, field programmable gate array (FPGA) control, movement and reading of the focusing stage, and inspection camera operation. A block diagram of the payload is shown in Figure 9, and a photograph of prototype electronics shown in Figure 10.

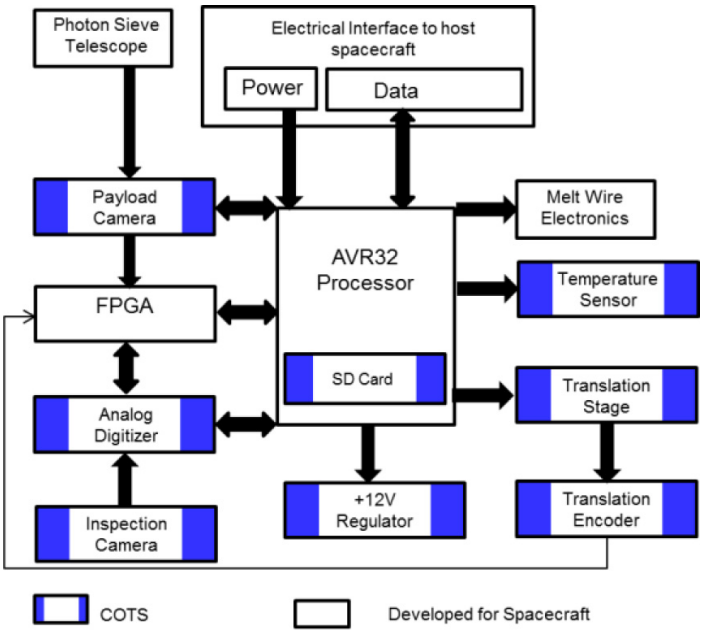

Figure 9. Payload electronics block diagram. Arrows indicate C&C signal flow.

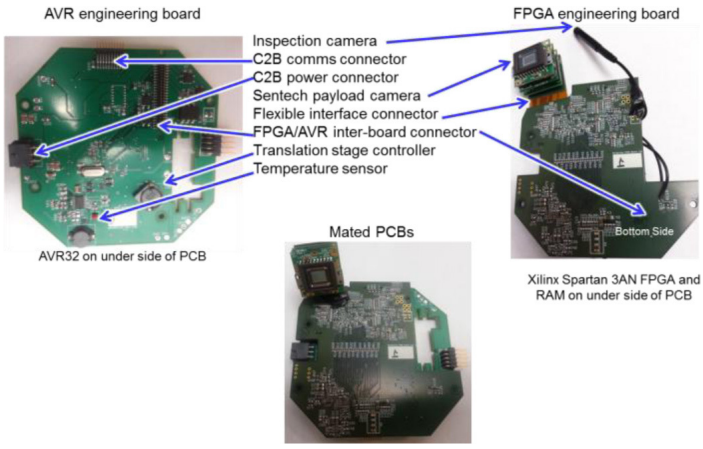

Figure 10. USAFA Peregrine prototype electronics boards.

Payload command and control electronics have been developed in-house. Some of the design has flown successfully on-orbit with other USAFA payloads (Balthazor, 2012; Stephani, 2013). The remainder has either been purchased as COTS (commercial off-the-shelf) components (some of which have had to be repackaged to fit in with the restrictive form factors for a CubeSat), or designed from scratch to FS-7 specifications.

An Atmel AVR32 microcontroller is the heart of the system. The AVR controls a Xilinx Spartan 3AN FPGA. The FPGA captures the digital images from the main camera at rates up to 19 frames per second, saves them to intermediate RAM, and provides a buffer for transmitting images back through the AVR to a 2 GB SD card used for flash storage. Each image is approximately 2.8 MB; thus, approximately 700 images can fit onto the 2 GB SD card. The FPGA can be configured on-orbit with the AVR. This is similar to what has been reported by the Jet Propulsion Laboratory for its COVE payload (Bekker, 2011). In addition to the functionality just described, the microcontroller also:

i) Operates the melt wire circuitry that activates the deployment system.

ii) Controls the main camera analog and digital gains, scanning, binning and exposure settings. The camera exposure time can be set anywhere from 10 microseconds and longer.

iii) Takes and downloads images, via a digitizer, from the inspection camera (a low-resolution camera positioned to verify that the deployment system has operated as designed).

iv) Drives and receives positional information from the focusing stage of the optical platform.

v) Communicates with the spacecraft bus on a 422 asynchronous bus.

The command and control electronics have been packaged onto two stacked printed circuit boards, each less than 82 x 82 mm in area and the stacked height less

than 1.5 cm.

With the help of NASA/Goddard, a trade analysis was conducted of ~20 cameras that potentially met physical and performance requirements, and the Sentech ST-152A CCD camera was selected. In addition to meeting requirements, use of this camera keeps mission cost low at the risk of using flight hardware that has not been space-rated. However, USAFA has a full suite of environmental testing facilities to include thermal-vacuum chambers, vibe tables, and plasma sources to simulate the space environment. Thermal-vacuum and vibration testing of the Sentech camera was performed (as part of the optical platform testing) to ensure it will be able to survive a nominal mission of three months on-orbit. Another advantage of using a commercial camera is that the control electronics for the camera are integrated with the camera itself, alleviating the requirement to develop new software for FPA access and control.

6. System Optical-Mechanical Modeling

Static and rudimentary dynamic modeling of Peregrine was conducted in the deployed configuration based on the expected on-orbit environment. Analysis of PS distortion attributable to disturbances from thermally induced vibrations by, and bulk temperature changes in, the pantographs, as well as vibrations induced by slew maneuvers have been completed. In addition to modeling, measurements were made of the vibrations induced by slew maneuvers (Eaton, 2013).

Finite element models of the pantographs were prepared for analysis using Finite Element Modeling and Postprocessing (FEMAP) version 10.2.0 (Stevens, 2012). All models were analyzed using MSC NASTRAN version 2008. As an example, Stevens' thermally induced vibration analysis is synopsized here. From thermal models, the steady state temperatures were mapped to the detailed FEMs of the pantograph legs. The temperatures were interpolated assuming symmetry and a "nearest" interpolation approach.

A static analysis was next performed on all of the detailed finite element models, using the steady state mapped temperature gradients as loads. The boundary grids of all models were constrained in all degrees of freedom. The constraint forces were recovered from each run, and were used as applied loads in the Peregrine assembly model.

The final analysis step in the process incorporates the data from the previous analyses into the Peregrine assembly model for use in a modal transient analysis. The forces were applied in the modal transient analysis by multiplying the steady-state forces and moments by a normalized exponential impulse function. A 0.1 second time constant was assumed, which is consistent with the thermal gradient found by thermal modeling.

The modal transient analysis was run using NASTRAN, by restarting from the pretensioned state solved in the nonlinear static analysis. The results were calculated using displacements relative to the initial pretensioned state. Key assumptions in the transient analysis are listed below.

- Retain all modes out to 100 Hz
- 0.1% modal damping (Bourgault & Miller, 2000)
- Spacecraft is rigid inboard of pantograph interface
- System is constrained at the interface
- System is linear under dynamic motion
  - No slip
  - Small displacements
  - Cables, sieve remain taut
- All results include a model uncertainty factor of 5.0

It was found that for all disturbances examined, the distortions of the PS were negligible compared to the expected PS positioning capabilities with the deployment structure, and that the relaxation time of the structure due to slewing was on the order of seconds. Relaxation times of the slew induced vibrations where confirmed by Eaton (2013).

Photometric analysis indicates that the SNR will be greater than 20 when looking at the Sun with a 100 microsecond integration time (Dearborn, 2012). It is relevant to note that for this PS telescope, a satellite with an unwanted slew of up to ~2 degrees/sec could be tolerated. This is approximately determined by ensuring the slew rate does not move the image plane at the Sun more than 4 μrad in 100 microseconds. In general, the camera is capable of integrating arbitrary times, so SNR is not expected to be an issue.

Finally, an opto-mechanical modeling procedure was completed to determine optical image performance. In short, this procedure followed a three step process:

1. Determine the positioning capability of the pantographs in the deployment system;

2. Use the positioning results in step 1) to generate in- and out-of-plane deformation of the photon sieve; and

3. Using Zemax, determine the effect on optical performance due to the deformations.

Based on mechanical design of the pantograph structure, the expected accuracy of the tip of the de-coupling springs (location of Point A) of the pantographs (shown in Figure 11) was analytically calculated. This was found to be a sphere of diameter 3.9 mm.

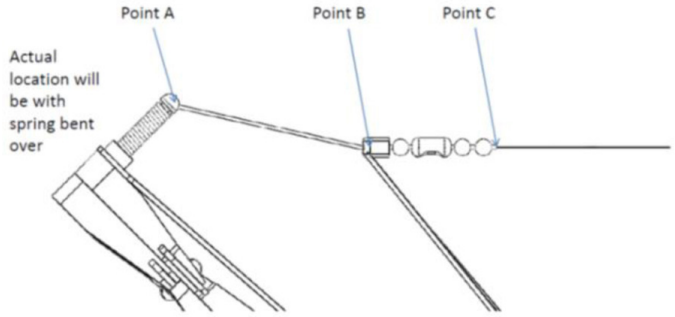

Figure 11. Side view of the pantograph, PS, and upper hexapod lanyards.

A finite element model of the PS, lanyards, and connectors to the PS and de-coupler springs was completed and run. From this model, the in-plane and out-of-plane deformations of the PS due to variations of the tips of the de-coupler springs (Point A) could be determined within the expected positioning accuracy. For example, Figure 12 shows out-of-plane deformations for one possible case of mis-alignment of the tips of the de-coupling springs. This case is expected to be the most stressing, because it gives the largest tilt of the PS. In addition to the in- and out-of-plane deformations, the tip/tilt and de-centering of the PS due to these mis-alignments were also determined, finding that these displacements have the greatest effect on the imaging performance of the telescope.

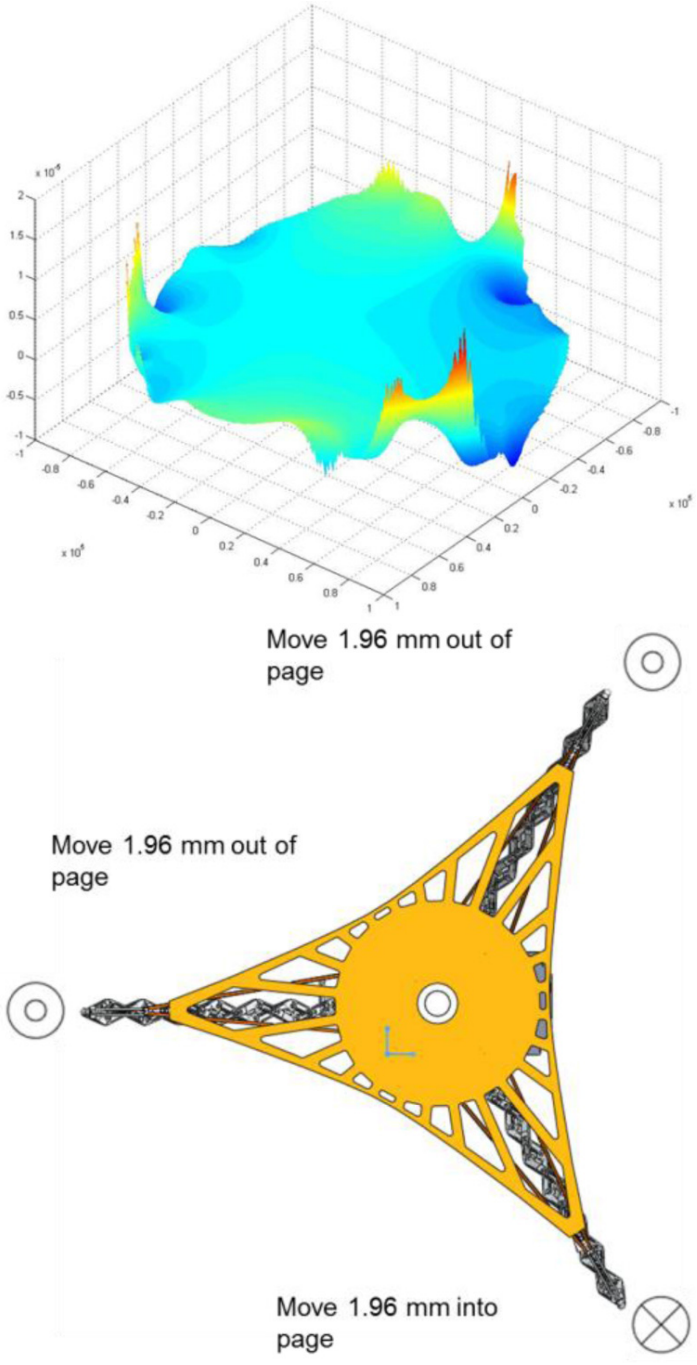

Figure 12. PS out-of-plane deformations (top) due to off-nominal positioning of the de-coupling springs as shown (bottom). Deformations shown in meters.

The top photograph in Figure 13 is an image of the Sun taken on 2012/07/31 and produced by Solar Dy-

namic Observatory (SDO) that is 0.14 degrees in angular size (or 0.59 arcsec/pixel) that has been modified for Peregrine performance. This image is a close match to FOV/resolution requirements for Peregrine's imaging capabilities (0.18 deg, 1360 x 1024 pixels, 0.48 arcsec/pixel), and is used for Peregrine telescope performance analysis. Modification of the image was due to PS deformations and misalignments incorporated into an optical model created in Zemax. The image results in diffraction-limited performance in the center section, and with degraded performance toward the edges, due mostly to the primary aberration coma. The coma here is not an inherent property of the PS, but would be present for any f/2 singlet lens. The bottom picture is the simulated image with the PS deformations due to misalignment of the tips of the de-coupling springs, as shown in the bottom of Figure 12, with best imaging performance at the center of the image 13 times diffraction limited.

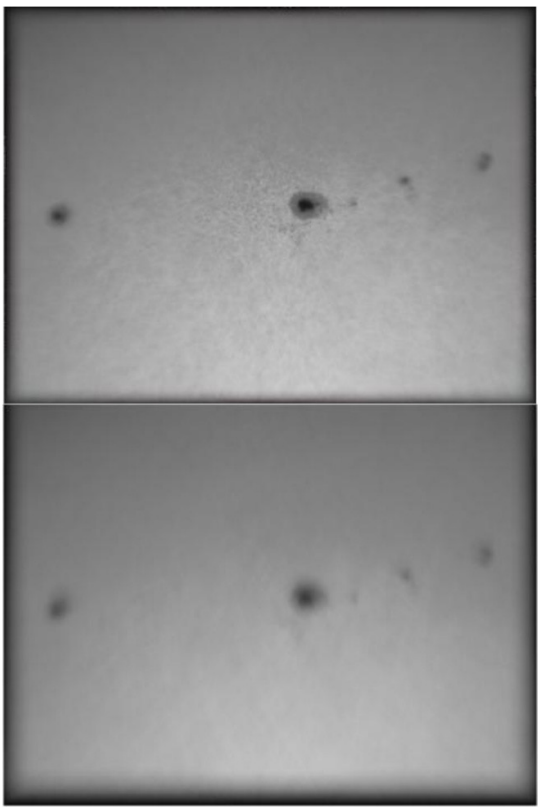

Figure 13. (Top) Peregrine simulated image with effects of system aberrations and distortions, but with the PS perfectly placed by the deployment structure. (Bottom) Peregrine simulated image with system aberrations, distortions, and deformations due to deployment as in Figure 12. Image area is 0.18 x 0.14 degrees.

7. Conclusions

The authors are now constructing and testing the Peregrine payload for integration with a 3U CubeSat. This payload will demonstrate the effectiveness of deployable membrane telescopes for imaging missions by taking pictures of the Sun. The PS technology can potentially be scaled to large apertures (up to twenty meters) and hosted on larger spacecraft. The majority of analysis of the payload has been completed, with the finding that it will provide acceptable imaging performance to demonstrate the technology. A CubeSat has been chosen as the satellite bus, since the low cost of CubeSats makes them ideal for testing technology. CubeSats are relatively easy to launch from a myriad of launch platforms, including both commercial launch companies specializing in small satellite launches and national launches, making them an ideal platform for a variety of imaging missions using the PS technology.

Acknowledgements

The authors wish to acknowledge support for this project from the Defense Advanced Research Projects Agency and the Department of Defense Space Test Program. Peregrine is a collaborative effort that includes participation from USAFA, HUA Inc., Space Scientific Instruments, Inc. (SSI), MMA Design Inc., NASA/GSFC, AFIT, AFOSR, and AFRL/RVSV. Special thanks are extended to Adrian Daw and Craig Stevens of NASA/GFSC, and Eric Swenson, Adrian Eaton, and Maggie Blackstun of AFIT.

References

Andersen, G. (2005): Large optical photon sieve, *Optics Letters*, Vol. 30, No. 22, November 15, 2005, pp. 2976-78.

Andersen, G. and Tullson, D. (2007): Broadband antihole photon sieve telescope, *Applied Optics*, Vol. 46, No. 18, June 20, 2007, pp. 3706-08.

Arsenault, H. (1968): Diffraction theory of Fresnel Zone Plates, *J Optical Society of Am*, Vol. 58, Issue 11, pp. 1536-1536 (1968).

Balthazor, R., et al. (2012): Measurements of the Ionosphere Using Miniaturized Electrostatic Analyzer on MISSE-7, presented at the *2012 National Space and Missile Materials Symposium*, Tampa, FL, June 2012.

Bekker, D., et al. (2011): The COVE Payload – A Reconfigurable FPGA-Based Processor for CubeSats, presented at the *25th AIAA Conference on Small Satellites*, 2011, paper SSC11-I-2.

Bourgault, F., and Miller, D. (2000): Model Uncertainty and Performance Analysis for Precision Controlled Space Structures. Massachusetts Institute of Technology, Department of Aeronautics and Astronautics.

Bleier, T., et al. (2004): QuakeSat: Low Cost University/Commercial Nanosatellite Collaboration, *CubeSat Developers Workshop*, CalPoly, San Luis Obispo, CA, USA, April 8-10, 2004.

Dearborn, M., et al. (2012): FalconSat-7: A Deployable Solar Telescope Mission, presented at the *International Astronautical Congress*, Naples, Italy, 2012, paper 12.B4.6B.1.

Eaton, A. (2013): Vibrational Analysis and Characterization of a Space-Based Deployable Photon Sieve, AFIT masters thesis, AFIT-GA-ENY-13-M-12.

Footdale, J., et al. (2013): Design and Testing of Self-Deploying Membrane Optic Support Structure Using Rollable Composite Tape Springs, presented at the *54th AIAA/ASME/ASCE/AHS/ASC Structures, Structural Dynamics, and Materials Conference*, paper AIAA 2013-1459.

Fuller, J., et al. (2010): CubeSat Balloon Drag Devices: Meeting the 25-Year De-Orbit, presented at the *2010 CubeSat Summer Workshop*, San Luis Obispo, CA, The Aerospace Corporation, August 2010.

Katan, C. (2012): NASA's Next Solar Sail: Lessons Learned from NanoSail - D2, presented at the *26th Annual AIAA/USU Conference on Small Satellites*, Logan, UT Aug. 2012.

Lites, B. (1991): The orbiting solar laboratory. The National Center for Atmospheric Research, Boulder, CO Advances in Space Research 01/1991; DOI:10.1016/0273-1177(91)90377-V.

Minelli, G., et al. (2008): Extended Life Flight Results from the GeneSat-1 Biological Microsatellite Mission, presented at the *2008 AIAA Conference on Small Satellites, Logan*, UT, AIAA Paper No. SSC08-II-4.

Niesel, D. (2010): PharmaSat: A Nanosatellite Platform for Biological Experimentation, presented at the 48th AIAA Aerospace Sciences Meeting Including the New Horizons Forum and Aerospace Exposition, 2010, Paper 10.2514/6.2010-736.

Simms, L., et al. (2012): Space-based telescopes for actionable refinement of ephemeris pathfinder mission, Optical Engineering, Volume 51, Issue 1, Jan. 19, 2012.

Stephani, K., et al. (2013): Analysis and Observation of Spacecraft Plume/Ionosphere Interactions during Maneuvers of the Space Shuttle, submitted to Journal of Geophysical Research.

Stevens, C. (2012): FalconSat-7 Peregrine Deployable System and Photon Sieve Performance Analysis, Goddard Space Flight Center informal report.

Stohlman, O. and Lappas, V. (2013): Deorbitsail: A Deployable Sail for De-orbiting, presented at the *54th AIAA/ASME/ASCE/AHS/ASC Structures, Structural Dynamics, and Materials Conference*, 2013, paper 10.2514/6.2013-1806.

VanHalle, R. (2013): De-Orbit Module, presented at the *National Space & Missile Materials Symposium*, Bellevue, WA, Jun 24, 2013.